EFDA–JET–PR(07)55

G. Vagliasindi, A. Murari, P.Arena, L.Fortuna, G. Mazzitelli
and JET EFDA contributors

Application of Cellular Neural Network Methods to Real Time Image Analysis in Plasma Fusion

Application of Cellular Neural Network Methods to Real Time Image Analysis in Plasma Fusion

G. Vagliasindi[1], A. Murari[2], P.Arena[1], L.Fortuna[1], G. Mazzitelli[3]
and JET EFDA contributors*

JET-EFDA, Culham Science Centre, OX14 3DB, Abingdon, UK

[1]Dipartimento di Ingegneria Elettrica Elettronica e dei Sistemi-Università degli Studi di Catania, 95125 Catania, Italy
[2]Consorzio RFX-Associazione EURATOM ENEA per la Fusione, I-35127 Padova, Italy.
[3]ENEA-Gestione Grandi Impianti Sperimentali, via E. Fermi 45, 00044 Frascati, Rome, Italy
** See annex of M.L. Watkins et al, "Overview of JET Results ", (Proc. 21 st IAEA Fusion Energy Conference, Chengdu, China (2006)).*

Preprint of Paper to be submitted for publication in
IEEE Transactions on Plasma Science

ABSTRACT.
In modern tokamaks visible and infrared video cameras are becoming more and more important to monitor plasma evolution during fusion experiments. Analyzing these images in real-time can provide relevant information for controlling the plasma and improving the safety of the machines. The real-time image processing capability of the Cellular Nonlinear Network based chip has been applied to several tasks both at Frascati Tokamak Upgrade (FTU) and Joint European Torus (JET). The successful applications range from the identification of plasma instabilities, such as Multifaceted Asymmetric Radiation From the Edge (MARFEs), to the determination of the strike points position in the divertor and the detection of hot spots.

1. INTRODUCTION

In the last years video cameras have been extensively used in magnetic confinement fusion experiments for both the understanding of the physics and the safety of the operation. Both visible and InfraRed (IR) images can be used not only to monitor the evolution of a plasma discharge but also to evaluate specific parameters, from the evolution of impurity radiation to the distribution of power loads on the plasma facing components. Data analysis is normally performed offline, due to the high amount of information to be processed, making the data acquired by the camera quantitatively useful only for post pulse studies. The main difficulty in using visible or infrared images for plasma feedback control is the fact that real-time image processing is challenging and heavy in terms of processing time, especially when complex tasks are required. Since digital image processing operates sequentially, it requires high clock frequencies to achieve acceptable performance for real time applications, with the consequent problems of consumption, signal integrity and so on. In order to overcome these issues the route of parallel processing has been investigate in JET and FTU using the approach of analog and mixed-mode circuits, like Cellular Nonlinear Networks (CNNs) [1] since they are particularly suited for fast computation. The CNNs are an array of simple, identical, locally interconnected nonlinear dynamic circuits called cells. Each cell interacts, via weighted connections, with the cells in the neighborhood of a limited radius. The analog implementation permits parallel processing at the hardware level of the individual pixels. Moreover, the CNNUniversal Machine paradigm [2] provides the capability to program and sequence in time the computational operations. In addition, it permits the storage of the intermediate results and can be implemented as a mixed-signal VLSI chip [3].

Several application of CNN-based hardware and software techniques were developed in the last years at FTU and JET, exploiting both the output of visible and infrared cameras. An overview of these algorithms is here reported together with a brief description of CNNs. The first application was to MARFE detection at FTU exploiting visible images in order to prevent disruptions due to excessive radiation emission. IR images were used at JET to determine the position of the strike-points, to complement the measurements of the magnetic coils, and to the early detection of hot spot, those points in the wall where the temperature approaches dangerous values. All these tasks were tested on the ACE16K CNN-based chip [4], a VLSI implementation of the CNN-UM paradigm. The chip is

able to process in a parallel way up to 16384 pixels, corresponding to a 128×128 image and to perform a linear convolution of 3×3 neighborhood on them in less than 3μs.

2. CELLULAR NONLINEAR NETWORKS

The concept of CNNs was introduced in 1988 by L.O. Chua [1]. The architecture of the CNN is made up of a basic circuit called cell, containing linear and nonlinear circuit elements (see Fig.1).

Each cell in a CNN is connected to its local neighboring cells, so a direct interaction occurs only among adjacent cells. An example of a two-dimensional CNN is shown in Fig.2. The neighborhood of the cell on the i-th row and j-th column, denoted by C(i, j), has the following definition:

$$N_r(i,j) = \{C(k,l) \mid \max\{|k-i|, |l-j|\} \le r, \} \quad 1 \le k \le M; \quad 1 \le l \le N \tag{1}$$

where r is a positive integer number, which fixes the dimension of the neighborhood.

A CNN is entirely characterized by a set of nonlinear differential equations associated with the cells in the circuit. Several mathematical model for the state equation of the single cell has been proposed since their introduction. The model as implemented in the CNN Universal chip family [3], also called Full Signal Range (FSR), is given by the following set of relations:

$$C_x \frac{dx_{ij}(t)}{dt} = -\frac{1}{R_x} g(x_{ij}(t)) + \sum_{C(k,l) \in N_r(i,j)} A(i,j;k,l) y_{kl}(t) + \sum_{C(k,l) \in N_r(i,j)} B(i,j;k,l) u_{kl}(t) + I \tag{2}$$

and the output equation is:

$$y_{ij}(t) = x_{ij}(t) \tag{3}$$

where *u*, *x*, and *y* denote the input, state, and output of the cell, respectively; R_x and C_x are the values of the linear resistor and linear capacitor, that determine the time constant of the circuit; *A(i, j; k, l)* and *B(i, j; k, l)* are the feedback and control templates respectively; *I* is the bias term, that is constant for all the CNN cells; *g(x)* is the nonlinear function in the state equation (2), depicted in Fig.3.

This last element is the main difference between the classical Chua-Yang CNN model [1] and the FSR model. In fact, in the former one, the nonlinearity enters into the output equation and is the integral of g(x). In [3] it has been demonstrated that the two mathematical models are equivalent.
processing. In this case the input image is mapped on the CNN in such a way that each image pixel is associated with the input or initial state of a particular cell. The CNN evolution implies a transformation of the input image into the corresponding output image obtained directly by the equation (2). In this contest, the template operators work like the instructions in a programming code. A huge amount of templates and template algorithms for a variety of tasks is already available in the literature [6].

The hardware prototype system used in this application is based on two fundamental parts: the CNN Universal Chip prototype, which is a 128×128 CNN chip [4], and the CNN Chip Prototyping and Development System (CCPS) platform [5]. The chip is mixed signal and is developed following the concept of Single Instruction Multiple Data (SIMD) architectures. It is named ACE16K, where ACE is the acronym of Analogic Cellular Engine to underline the mixed signal nature of the chip (analogue and logic) and the fact that it is composed of 16K cells.

ACE16K can be described basically as an array of 128×128 identical, locally interacting, analog processing units designed for high speed image processing tasks requiring moderate accuracy (around 8bits). The system contains a set of on-chip peripheral circuitries that, on one hand, allow a completely digital interface with the host, and on the other hand provide high algorithmic capability by means of conventional programming memories where the algorithms are stored.

Although ACE16K is essentially an analog processor (computation is carried out in the analog domain), it can be operated in a fully digital environment. For this purpose, the prototype incorporates a bank of Digital-to-Analog (for input) and Analog-to-Digital (for output) converters at the images I/O port. ACE16K is conceived for use in two alternative ways. First, in applications where the images to be processed are directly acquired by the optical input module of the chip, and secondly, as a conventional image co-processor working in parallel with a digital hosting system that provides and receives the images in electrical form. The second mode of operation is the one adopted to obtain the results presented in this paper.

3. CNNS FOR MARFE DETECTION AT FTU

The first application of CNNs to plasma fusion field was the MARFE detection at FTU [7]. The MARFE [8] is a radiation instability which appears in tokamaks as a toroidally symmetric ring of increased radiation. It usually occurs on the inner side of the torus. The plasma is locally cooled by radiation leading to a self sustained process in which the decrease in temperature enhances the radiation losses resulting in further cooling. The principal reason is due to line radiation from impurities that increases with decreasing temperature.

This instability appears at high density and near the Greenwald limit [9]. After the onset of a MARFE further gas puffing does not lead to an increase of the electron density; moreover strong gas puffing into the discharge with a MARFE leads to a detached plasma or to a hard disruptions. In the first case it can be asserted that MARFEs represents a limit to the maximum attainable density but the second one, i.e. the disruption, is a dramatic event in which the plasma confinement is suddenly destroyed. In few milliseconds the current goes to zero and this leads to a large mechanical stress and to intense heat loads.

As a consequence it appears that real time control of MARFEs would be a useful mean to extend the plasma operation parameters and to avoid dangerous disruption. Camera observations of a wide poloidal portion of the plasma edge represent a good candidate for early detection of the MARFE onset and the development of a feedback control in order to mitigate its effects.

The idea is, once detected a MARFE in the tokamak, to stop immediately the gas puffing and then to move the plasma column in order to modify, in that region, thermal conduction both parallel and perpendicular to the magnetic field. In this way control of the growth rate of MARFEs should be achieved at least early enough to avoid disruptions.

A preliminary work has been dedicated to translate the physical information about the MARFE in visual features revealable in the images captured by the video monitoring system. The set of visual parameters which has been considered to be representative of the MARFE formation and its speed displacement are brightness, shape and velocity of its growing (see Fig.4).

A further analysis phase revealed that the shape of the MARFE is that of a very stretched ellipse, oriented in a diagonal direction. These last two visual features obviously depend on the position and tilt of the camera, but they can be considered invariant in this application, since the camera is installed with a fixed position and orientation.

An algorithm has been devised in order to monitor this visual parameters (see Fig.5). After the extraction of the frame from the video, an inversion operation is performed to obtain the negative frame. This is necessary since the CNNUM works in a grayscale that is inverted with respect to the usual image processing software. Subsequently, thresholding is performed to detect the pixel exceeding a given brightness. At this point, a DIAG1LIU [6] template is applied for detecting diagonal lines laying in the SW-NE direction.

This operation performs a control on the shape of the black object which, in this case, is an ellipse oriented along a diagonal (SW-NE) direction. Once identified the object shape and orientation, the following step consists of performing a check on its growing speed. This can be achieved observing the difference between two consecutive frames that gives an information about the dynamic evolution of the phenomenon. The number of pixels in the difference is evaluated, and in the case it exceeds a given threshold size, a warning message is shown. A detailed description of the algorithm is reported in [9].

The whole algorithm has been implemented on the CNN based chip ACE16K, available in the laboratories of the DIEES-University of Catania. Many videos were analyzed to carry out an algorithm with a high robustness respect to variations on the camera tilt.

The results obtained are shown in Fig.6 where the elaboration of two consecutive frames is presented. Only the portion of the whole frame (Fig.4) which includes the toroidal limiter was processed in order to minimize the execution time. It is possible to observe that a MARFE is detected and a warning message “Alert” appears, as can be appreciated in the upper right corner of this figure. During the processing, from this moment on, the warning message will be held on the screen, if the MARFE moves or increases.

The video monitoring system installed at FTU and used in this work operates at a temporal resolution of 25 frames/s which is doubled splitting the interlaced TV fields [12]. Indeed, the two half frame are interpolated providing, in this way, a frame every 20ms. The time, instead, to process two consecutive frames is about 13 ms, which is below the interframe rate. This real time detection system can help in

carrying out a safe conclusion of the experiment when the probability of the occurrence of a disruption is high, thus preventing the tokamak from mechanical and thermal stresses.

4. CNNS FOR STRIKE POINTS DETECTION

In Tokamak plasmas, the divertor is the region of the vacuum vessel explicitly designed to handle power losses. In JET history several topological solutions have been tested as far as the divertor is concerned.

The one used for the discharges, whose results are reported in this paper, is shown schematically in Fig.7. The typical Xpoint plasma configuration is also shown: it is characterized by the existence of a separatrix and a scrape-off layer. The former is the last closed flux surface that separates the closed magnetic field lines from the open ones which strike the vacuum vessel, while the latter is the region of the plasma where the magnetic field lines intersect wall elements, in this case the divertor. The plasma power losses are deposited along this region. The intersection of the separatrix with the divertor target plates represents a strike point.

In JET the position of the strike points is mainly derived from magnetic measurements performed with loops and pickup coils located around the vacuum vessel. These measurements, taken at some distance from the plasma, can be extrapolated across the current-free region to identify the last closed flux surface. The code used at JET to determine the plasma shape and therefore also the position of the strike points is XLOC [13]. The main output of XLOC consists of the definition of the last closed flux surface, also called separatrix.

In JET divertor various thermocouples are also located in the divertor tiles, covering the whole region were the magnetic field lines can intersect material surfaces. The region of maximum thermal load, which can be considered as the position of the strike points, can be identified thanks to thermocouple signals.

Another very useful diagnostic to derive information about the power deposition in the JET divertor is represented by infrared imaging. At the time of the experiments, two IR cameras framing the divertor region were available at JET. They measured the infrared radiation in the interval 3-5 ^{o}m with a resolution of 128×128 pixels [14].

One camera sees the outer leg of the divertor, the other the inner leg and, as far as real timecontrol is concerned, the two views can be considered representative of the entire divertor, given the toroidal symmetry of the machine. Also in this case, a preliminary analysis was necessary to determine how the presence of the strike points reflects itself in the visual features of the camera images. The strike points, indeed, can also be considered the region of maximum thermal load on the divertor tiles that is translated in an infrared image as the region of maximum brightness. A first manual analysis of images from JET IR cameras proved that the shape of the strike points consists of two thin bands of high emission in the whole divertor region, oriented in the toroidal direction.

A specific procedure was developed to derive the position of the strike points from the data of the infrared cameras exploiting the capabilities of CNN technology (see Fig.8).

The algorithm has been applied to a frame which is the composition of the two images covering respectively the inner and the outer side of the divertor region. These images should have really different brightness, which varies according to the different temperature the strike points reach in the two regions of the divertor. So it is necessary to perform an independent processing procedure for each one of them.

After an initialization step during which all the constants like threshold values, counter limits and so on are initialized, an inversion operation is performed. Subsequently, a THRESHOLD template is applied to the image, to identify the pixels whose value is higher than a predefined level. The result of this first processing phase is a binary image, where the black pixels represent those exceeding a given brightness threshold. In order to perform the independent processing of the two strike points, at this stage an AND operation with a mask is executed to select the pixels representing the inner or outer strike points. Then the number of remaining pixels in the image is evaluated to verify that it is adequate to perform the identification of the strike-point position. If it is less than a given number K, the threshold value in the THRESHOLD template is decreased by a constant value j, and the cycle is repeated. Otherwise the loop stops when the K value is reached.

The output of the algorithm at this stage consists of a band of black pixels, corresponding to the region of maximum brightness in the divertor legs. A SKELETONIZATIONtemplate is, then, applied to find the skeleton of the band. Once the skeleton of the inner strike point is obtained, the algorithm is executed once again, this time to extract the outer strike-point position.

The algorithm is capable of supplying the position of both the inner and the outer strike points within 20 ms. In particular, the time to identify the strike points in the image is comprised between 13 and 19 ms, depending on the brightness condition of the starting frame. This time resolution is acceptable for the vast majority of JET applications. It is indeed necessary to consider that in general the thermal phenomena, which can affect the tile temperature and change infrared emission, do not change much on shorter time scales.

In order to assess the accuracy of the proposed approach, a systematic comparison with the results of XLOC and the thermocouples measurement was undertaken (see Fig.9 and 10). To this end the co-ordinates of the strike points obtained with the CNN were compared with the ones given by XLOC, from the intersection of the separatrix with the divertor, and with the position of maximum load as given by the thermocouples. A good congruity between CNN and XLOC calculated strike points is noticed. The fact that CNN detects the maximum power load which is not always coincident with the intersection of the separatrix with the divertor is confirmed by the comparison with the thermocouple.

A further statistical comparison between the CNN estimate and the one derived from the magnetic reconstruction of the boundary was performed. In Fig. 11, the x axis shows the position calculated with the CNN approach, while the y axis reports the interception with the divertor of the flux line 5mm outside the separatrix calculated via the EFIT software [15].

The congruity between the two results is good: it can be noticed that the absolute error is included in the range [−1 cm: +1 cm] apart from some sporadic points.

5. CNNS FOR HOT SPOT DETECTION

Another application of IR imaging and CNN-based image processing is the early detection of hot-spots [16]. One of the future ITER relevant enhancement at JET will be the installation of a Beryllium wall. Since Be is much more vulnerable than stainless steel (the present JET's wall material), preserving the integrity of the plasma facing components will be one of the main issues in future JET experiments.

Detecting in real time the presence of hot spots, i.e. regions of the first wall where the temperature approaches dangerous levels, is considered crucial in the safety strategy as they are considered naturally the points more prone to significant damage. CNN technology has been therefore applied to the real time identification of hot spots.

Analyzing the data from JET cameras [17], it is possible to identify three main sources of anomalously high emission in the infrared region of the spectrum in JET (see Fig.12). Some parts of the vacuum vessel, like the limiters of the target plates, can reach very high temperatures, because they are the region were most of the plasma wall interactions take place in normal conditions.

These locations will have to be monitored continuously once JET new wall is installed to both understand the behavior of the materials and to guarantee safe operation of the device.

On the other hand, these regions are designed to withstand high energy fluxes and therefore specific thresholds will have to be used for them. Moreover their position and shape are fixed and therefore their monitoring relatively straightforward. A different emission is produced when other parts of the first wall, not meant to absorb a lot of energy, are subject to strong heating in case of unforeseen events, like disruptions, ELMs or errors in the set up of the magnetic configuration. The shape of these hot spots can be very different and their location inside the viewing cone of the camera quite unpredictable. Moreover their position can change during the discharge.

Particularly during fast events like ELMs and disruptions, a third type of IR emission can be due to particles ejected from the first wall and entering into the plasma. If they are big enough not to be immediately vaporized, struck by the plasma they can reach high temperatures and be clearly detected in the IR images. They have normally relatively small dimensions and fast changing position inside the field of view.

Taking into account the different nature of these IR emissions two different types of algorithms for the identification of the hot spots were developed. The first one, for the so called static detection, performs the analysis of a single frame at the time. It is more suited to the monitoring of the fixed parts of the machines, like the plasma facing components (limiters and divertor). A second approach, called dynamic detection, is based on the difference between subsequent frames. The latter algorithms are more complicated but they allow to follow the growth of the hot spots and their movements inside the field of view. Two examples of the proposed approaches are reported in Fig.13 while a detailed description is available in [16].

Both algorithms were tested using frames acquired by JET wide angle IR camera (KL7). As parts of the image are not relevant to the end of detecting hot spots (because they include regions of

the vessel not in contact with the plasma), the frame was cropped before processing it in order to speed up the processing.

The image is so reduced to a 384×384, eliminating also the portion of the frame, which sees the divertor as there is already another infrared camera (KL3) that monitors this part of the machine with greater accuracy. An example of the result produced by the static algorithm is reported in Fig.14. The contour of the detected regions is superimposed to the starting frame. It is possible to observe that they represent the point of maximum brightness assimilable, at this step, to the hottest point in the vessel. The execution times for both the algorithms are reported in Table II. The execution time is in the order of 100ms to process the whole 384×384 frame. The time required to process only a 128x128 subframe is about of 20ms. This higher time resolution could be very helpful for machine protection. For instance, particularly delicate parts of the machine, like the RF antennas, which occupy a region of the image not wider than two 128×128 images, could be monitored with a high time resolution.

CONCLUSIONS

The visible and infrared emission contains a lot of useful information exploitable for plasma monitoring to enhance the performance or the safety of tokamak machines. The data provided by visible and infrared cameras installed at FTU and JET were processed in order to monitor dangerous plasma phenomena, like MARFE or hot spots, or to extract relevant parameter like the maximum thermal load position in the divertor. To take advantage of the potentialities of CNNs, several algorithms were devised to perform the previously mentioned tasks. Thanks to the capabilities of ACE16K, a VLSI implementation of CNNs, the processing time for the various tasks is below the inter-frame rate.

The algorithms described in this paper represent the first application of CNNs to fusion experiments. Further investigation is going to be performed in order to assess the potential of CNN technology in the real time environments of reactor tokamaks.

ACKNOWLEDGMENTS

The work was partially supported by the Project “Realtime visual feature extraction from plasma experiments for real time control,” funded by ENEA-EURATOM.

REFERENCES

[1]. L.O. Chua, L. Yang, “Cellular Neural Networks: Theory and Applications”, *IEEE Trans. Circuits and Systems-part I*, **35**, pp. 1257-1290, 1988.

[2]. L.O. Chua, K.R. Crounse, “The CNN Universal Machine is as Universal as a Turing Machine”, *IEEE Trans. On CAS-I*, vol. **53**, no.4, April 1996.

[3]. S. Espejo et al., “A VLSI-Oriented Continous-Time CNN Model”. *International Journal of Circuit Theory and Applications*. Vol. **24**, pp 341-356, May-June 1996.

[4]. A. Rodríguez-Vázquez, el al. ,”ACE16K: The Third Generation of Mixed-Signal SIMD-CNN ACE Chip Toward VSoCs”, *IEEE Transaction on Circuits and Systems-I:REGULAR PAPER*, Vol.**51**, no.5, May 2004

[5]. A. Zaràndy, T. Roska, P. Szolgay, S. Zöld, P. Földesy and I. Petràs, “CNN Chip Prototyping and Development Systems”, *European Conference on Circuit Theory and Design – ECCTD’99*, Design Automation Day proceedings, pp. 69-81. (ECCTD’99-DAD), Stresa, Italy, 1999.

[6]. T. Roska et al., CNN Software Library (Template and Algorithms) Version 7.3, Hungarian Academy of sciences ed. Budapest, Hungary: Computer and Automation Institute, 1999.

[7]. P. Arena et al, “Real time monitoring of radiation instabilities in TOKAMAK machines via CNNs”, *IEEE Transaction on Plasma Science*, Vol. **33**, Issue 3, June 2005, pp. 1-9.

[8]. B. Lipschultz, “Marfe: an edge plasma phenomenon,” *Nuclear Fusion*, vol **24**, n 8, Aug. 1984, p 977-89

[9]. M. Greenwald, “A new look at density limits in Tokamaks,” Nuclear Fusion, vol **28**, n 12, Dec. 1988, p. 199-207

[10]. http://onyx2ced.frascati.enea.it/videoftu/Movies

[11]. P. Arena et al., “Cellular Nonlinear Networks For Strike-Points Localization At JET”, *Rev. Sci. Instrum.* **76**, Issue 11, Article 113503 (November 2005).

[12]. R. De Angelis et al., “Analysis of images from videocameras in the Frascati Tokamak Upgrade tokamak”, *Rev. Sci. Instrum.* **75**, Issue 10, pp. 4082-4084, October 2004.

[13]. F. Sartori, A. Cenedese and F. Milani, “JET real-time object-oriented code for plasma boundary reconstruction”, *Fusion Eng. Des.*, vol. **66-68**, pp. 735-739, 2003.

[14]. V Riccardo et al, “Disruption heat loads on the JET MkIIGB divertor”, *Plasma Phys. Control. Fusion*, vol. **44**, pp. 905-929, 2002.

[15]. L.L. Lao et al., Reconstruction of current profile parameters and plasma shapes in tokamaks. *Nucl. Fusion 25*, p. 1611, (1985).

[16]. G. Vagliasindi, A. Murari, P. Arena, G. Arnoux, L. Fortuna, E. Gauthier, “First Application of Cellular Neural Network Methods to the real time identification of Hot Spots in JET”, under review.

[17]. E. Gauthier et al., “ITER-like wide-angle infrared thermography and visible observation diagnostic using reflective optics”, 24th Symposium on Fusion Technology (SOFT 2006), 11-15 September 2006, Warsaw, Poland, to be published in Fusion Engineering and Design.

[18]. G. Vagliasindi et al, “Application of Cellular Neural Network Methods to Real Time Image Analysis in Plasma Fusion”, Proceedings of the 2007 IEEE Symposium on Intelligent Signal Processing, WISP07, 3-5 October 2007, Alcalà de Henares, Madrid, Spain, pp. 967-972.

OPERATION	TIME (ms)
Inner strike detection	7 - 10ms
Outer strike detection	6 - 9ms
TOTAL	**13 – 19ms**

TABLE I.
Execution time for strike point detection algorithm

ALGORITHM	TIME (ms)
Static Detection (full frame)	~ 56 ms
Dynamic Detection (full frame)	~ 58 ms
Static Detection (128×128)	~ 8 ms
Dynamic Detection (128×128)	~ 8 ms

TABLE II.
Execution times for the static and dynamic algorithm applied to a full frame or a 128×128 subframe.

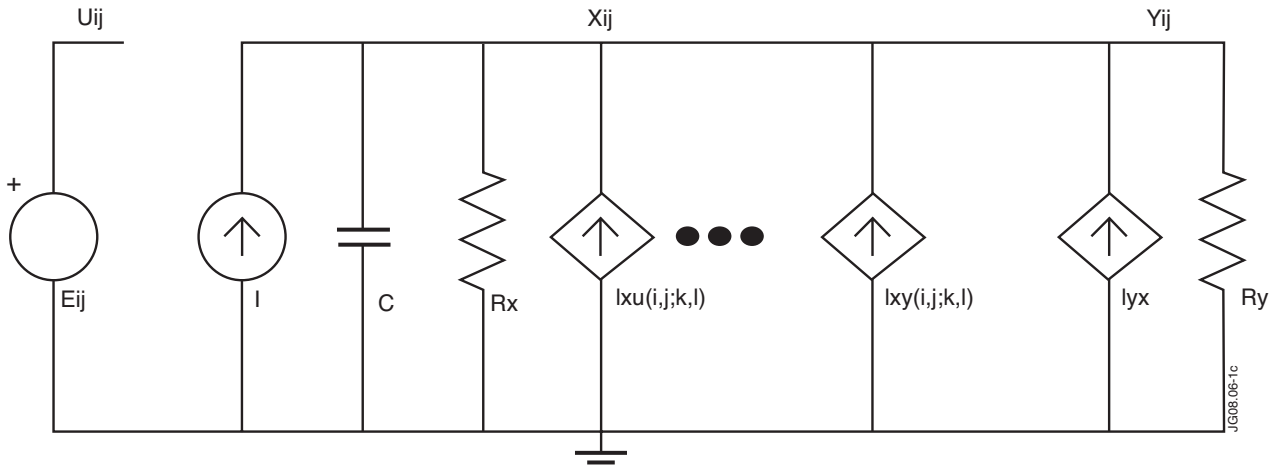

Figure 1: The Chua-Yang *cell circuit model*

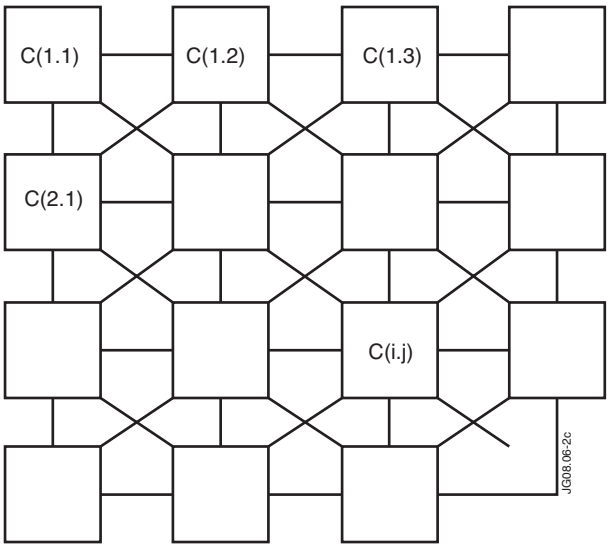

Figure 2: An example of a two dimensional CNN

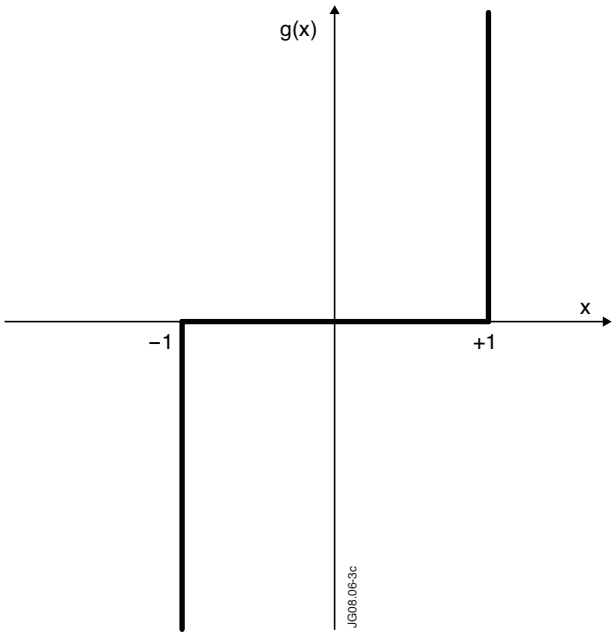

Figure 3: Nonlinear function in the Full Signal Range CNN model, as implemented in the CNN chip One of the main applications of CNNs is image

Figure 4: Example of MARFE growing from FTU Pulse No: 22214

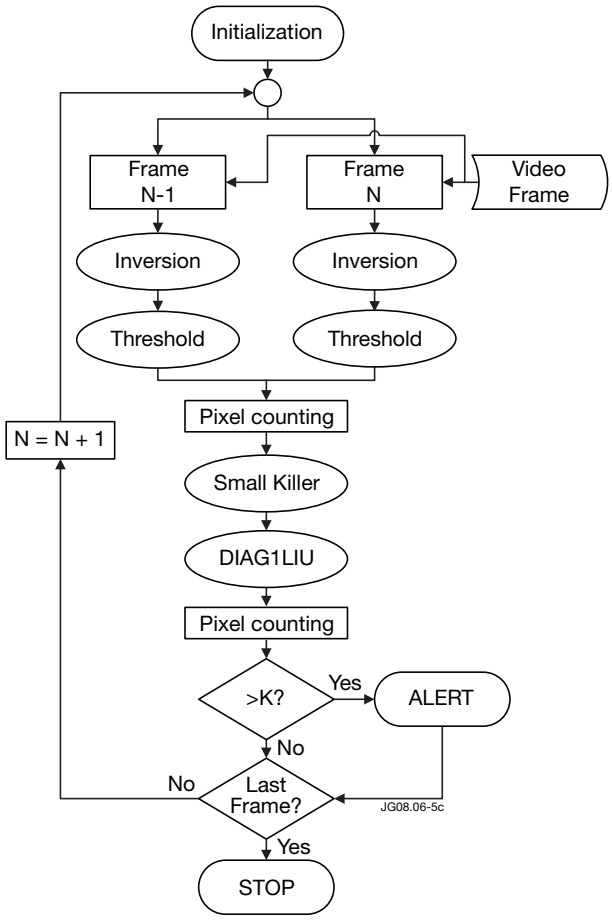

Figure 5: Flowchart of the algorithm for real time MARFE detection. The steps in the ellipses represent template operations.

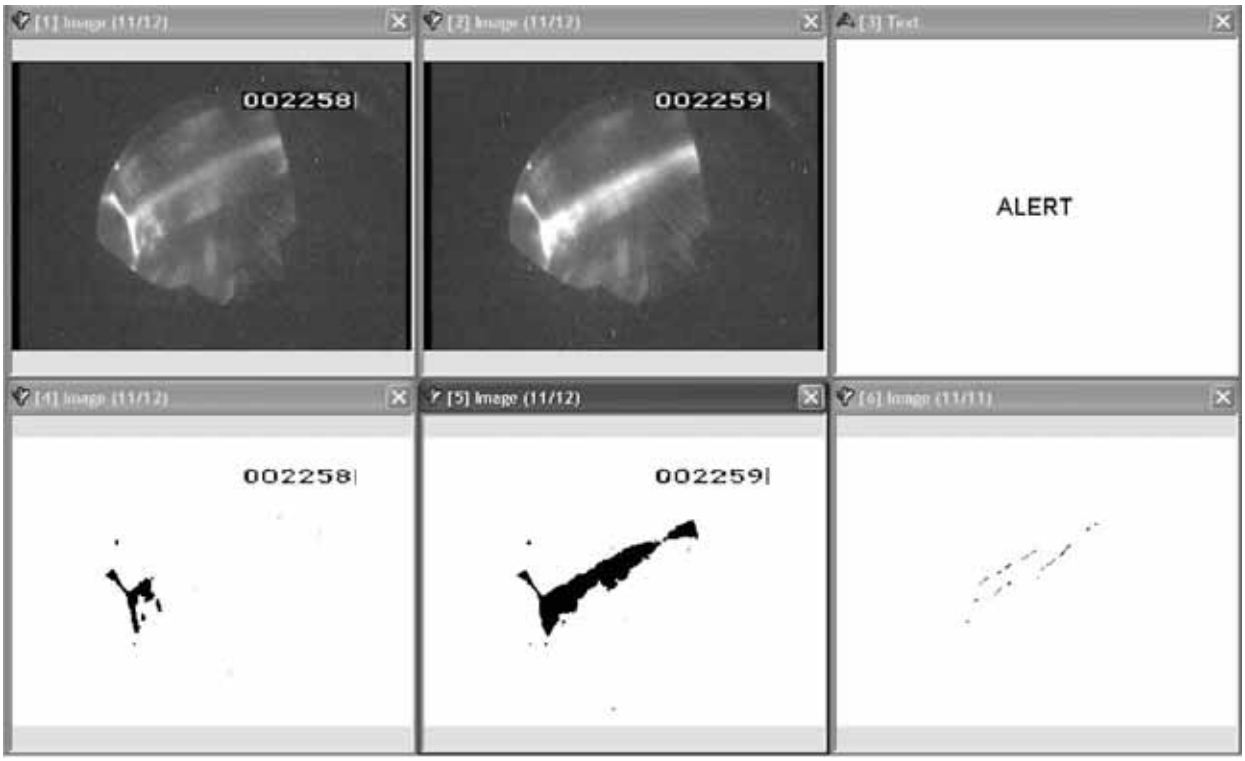

Figure 6: an elaboration of two consecutive frame (2258, 2259) from Pulse No: 22214. It is possible to observe in the upper-right frame the message ALERT caused by a MARFE, whose shape can be noticed in the lower frames [9].

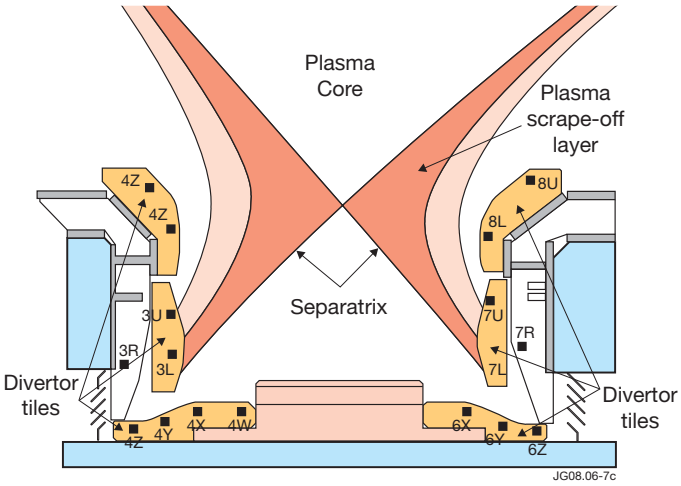

Figure 7: A schematic outline of JET divertor topology. The black squares represent the thermocouples position.

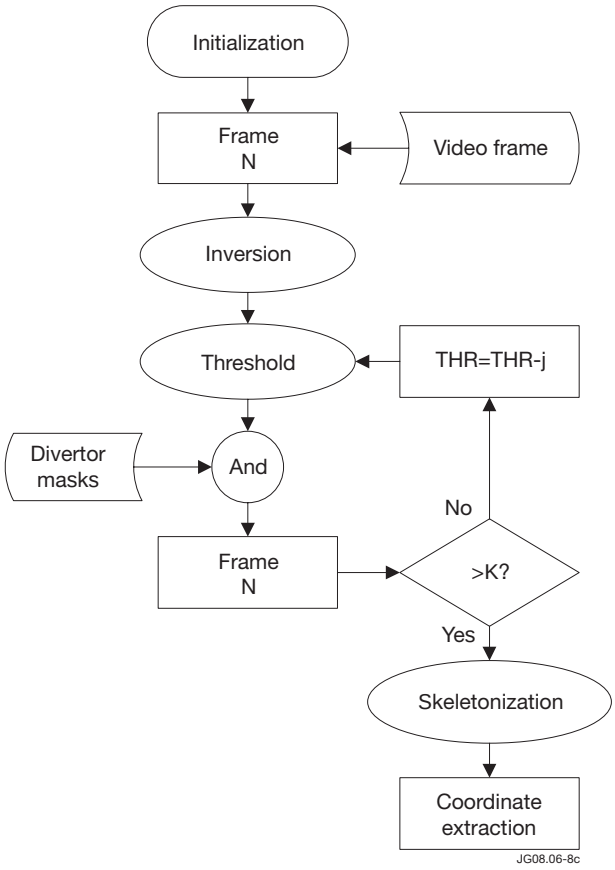

Figure 8: Flowchart of the algorithm for strike point detection at JET.

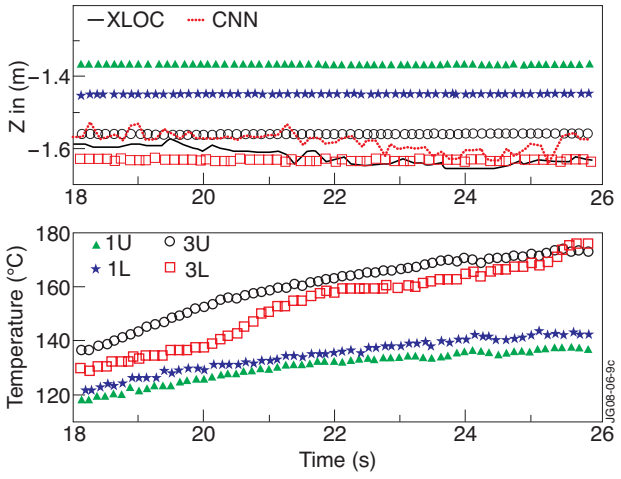

Figure 9: In the top figure, the time evolution of the CNN and XLOC calculated strike points is shown, together with the coordinate Z of the available thermocouples in the inner part of the divertor. In the bottom figure, the time evolution of the thermocouples temperature is shown (Pulse No: 62216) [11].

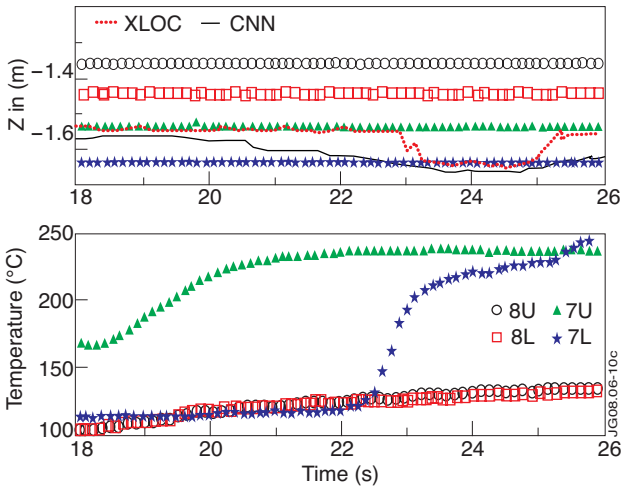

Figure 10: In the top figure, the time evolution of the CNN and XLOC calculated strike points is shown, together with the coordinate Z of the available thermocouples in the outer part of the divertor. In the bottom figure, the time evolution of the thermocouples temperature is shown (Pulse No: 62216) [11] .

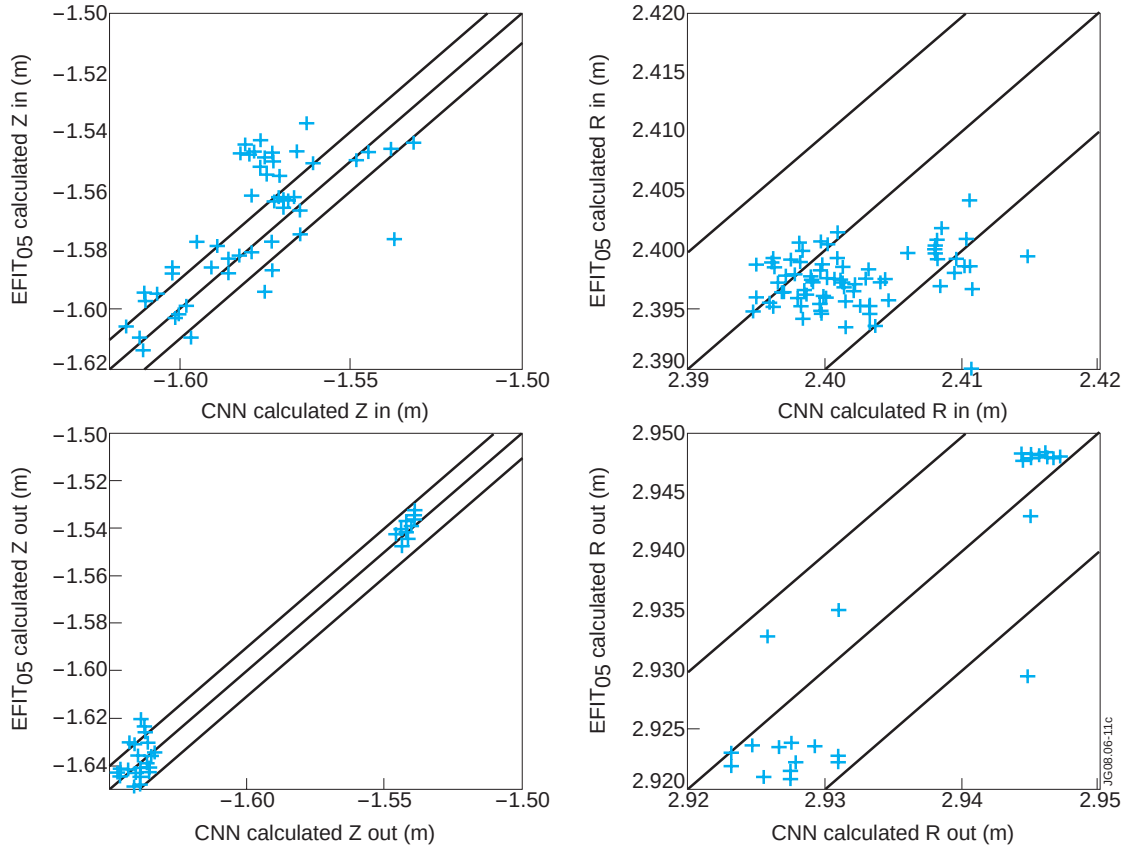

Figure 11: Comparison of the R and Z estimate of the strike points as derived from the CNN and EFIT05. The line in the middle represent a perfect agreement among the measurements while the other two lines defines the interval [−1cm : +1cm].

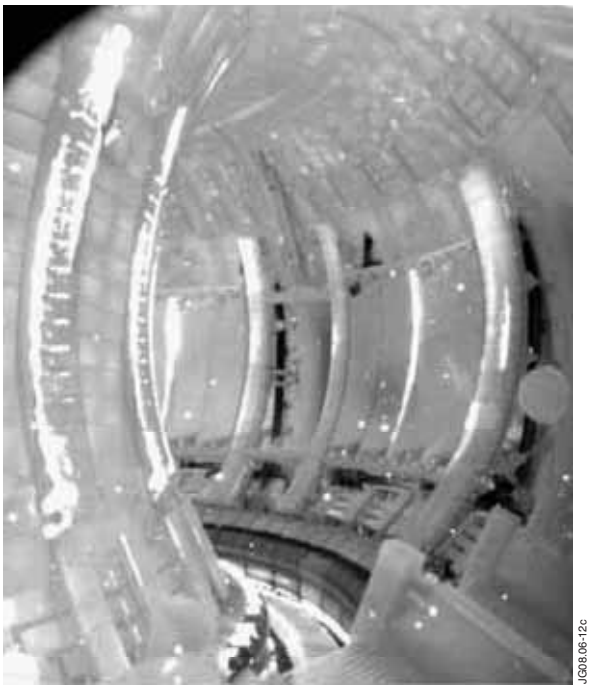

Figure 12: Example of the three main types of hot spots as seen with JET wide angle IR camera. (Pulse No: 66503). The smallest circular bright spots are particles entering the plasma. The big crescent shape bright regions are on the limiters, locations designed to withstand high powers. Some smaller bright spots on the top are due to plasma wall interactions changing fast with time.

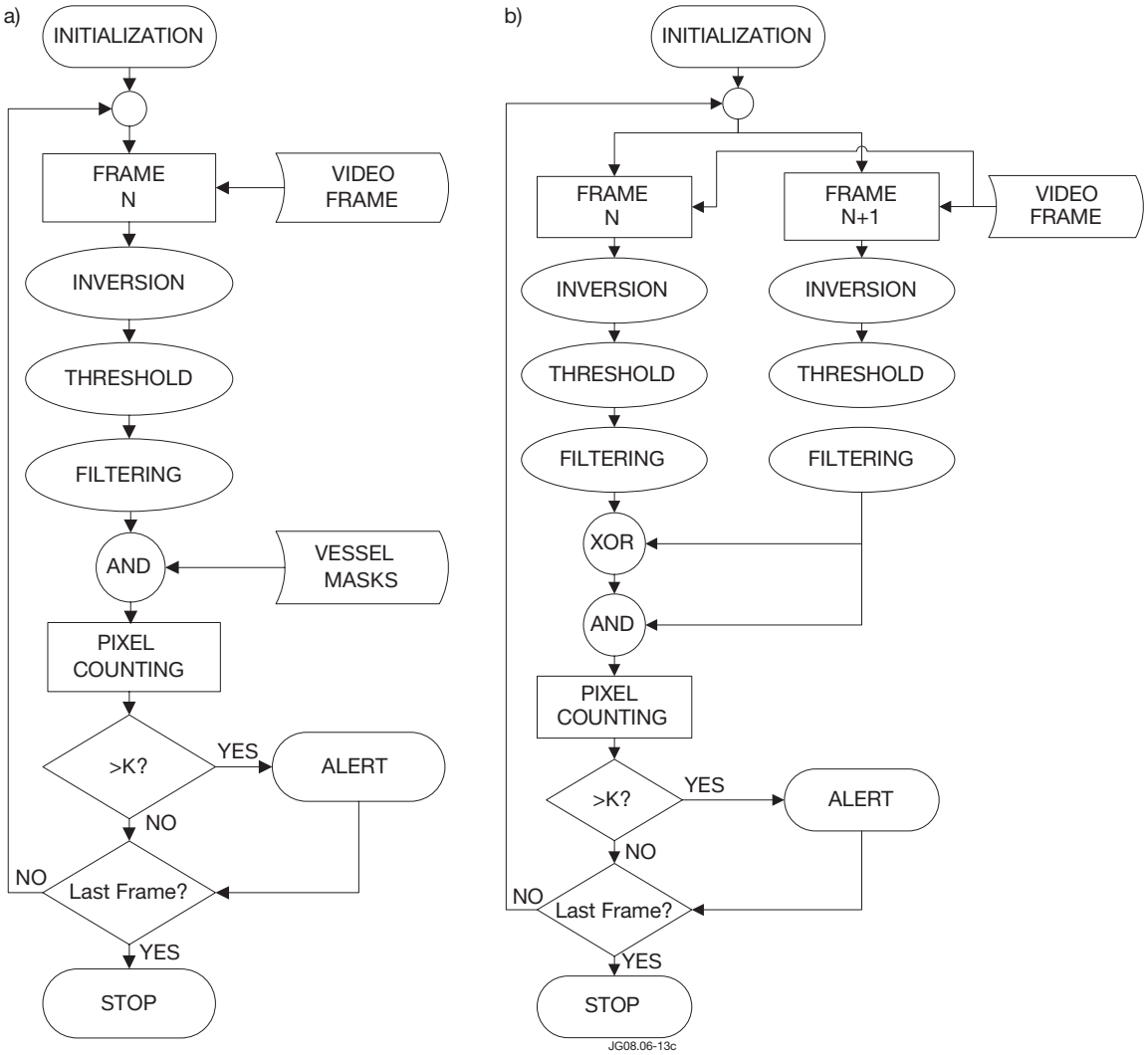

Figure 13: Flowchart of the algorithm for the identification of the hot spots: a) static version, b) dynamic version.

Figure 14: Example of static detection of hot spots. The contour of the detected regions is reported superimposed to the starting frame.